NASA/TP-20205011711

Effect of Reactant Purity on Proton Exchange Membrane Fuel Cell Performance

Phillip J. Smith, William R. Bennett, Ryan P. Gilligan, Ian J. Jakupca
Glenn Research Center, Cleveland, Ohio

July 2021

NASA STI Program . . . in Profile

Since its founding, NASA has been dedicated to the advancement of aeronautics and space science. The NASA Scientific and Technical Information (STI) Program plays a key part in helping NASA maintain this important role.

The NASA STI Program operates under the auspices of the Agency Chief Information Officer. It collects, organizes, provides for archiving, and disseminates NASA's STI. The NASA STI Program provides access to the NASA Technical Report Server—Registered (NTRS Reg) and NASA Technical Report Server—Public (NTRS) thus providing one of the largest collections of aeronautical and space science STI in the world. Results are published in both non-NASA channels and by NASA in the NASA STI Report Series, which includes the following report types:

- TECHNICAL PUBLICATION. Reports of completed research or a major significant phase of research that present the results of NASA programs and include extensive data or theoretical analysis. Includes compilations of significant scientific and technical data and information deemed to be of continuing reference value. NASA counter-part of peer-reviewed formal professional papers, but has less stringent limitations on manuscript length and extent of graphic presentations.

- TECHNICAL MEMORANDUM. Scientific and technical findings that are preliminary or of specialized interest, e.g., "quick-release" reports, working papers, and bibliographies that contain minimal annotation. Does not contain extensive analysis.

- CONTRACTOR REPORT. Scientific and technical findings by NASA-sponsored contractors and grantees.

- CONFERENCE PUBLICATION. Collected papers from scientific and technical conferences, symposia, seminars, or other meetings sponsored or co-sponsored by NASA.

- SPECIAL PUBLICATION. Scientific, technical, or historical information from NASA programs, projects, and missions, often concerned with subjects having substantial public interest.

- TECHNICAL TRANSLATION. English-language translations of foreign scientific and technical material pertinent to NASA's mission.

For more information about the NASA STI program, see the following:

- Access the NASA STI program home page at http://www.sti.nasa.gov

- E-mail your question to help@sti.nasa.gov

- Fax your question to the NASA STI Information Desk at 757-864-6500

- Telephone the NASA STI Information Desk at 757-864-9658

- Write to:
  NASA STI Program
  Mail Stop 148
  NASA Langley Research Center
  Hampton, VA 23681-2199

NASA/TP-20205011711

Effect of Reactant Purity on Proton Exchange Membrane Fuel Cell Performance

Phillip J. Smith, William R. Bennett, Ryan P. Gilligan, Ian J. Jakupca
Glenn Research Center, Cleveland, Ohio

National Aeronautics and
Space Administration

Glenn Research Center
Cleveland, Ohio 44135

July 2021

Acknowledgments

The authors would like to thank Monica Guzik and Karin Bozak of NASA Glenn Research Center for their support in this effort.

Trade names and trademarks are used in this report for identification only. Their usage does not constitute an official endorsement, either expressed or implied, by the National Aeronautics and Space Administration.

Level of Review: This material has been technically reviewed by expert reviewer(s).

Available from

NASA STI Program
Mail Stop 148
NASA Langley Research Center
Hampton, VA 23681-2199

National Technical Information Service
5285 Port Royal Road
Springfield, VA 22161
703-605-6000

This report is available in electronic form at http://www.sti.nasa.gov/ and http://ntrs.nasa.gov/

Contents

Effect of Reactant Purity on Proton Exchange Membrane Fuel Cell Performance

Phillip J. Smith, William R. Bennett, Ryan P. Gilligan, Ian J. Jakupca
National Aeronautics and Space Administration
Glenn Research Center
Cleveland, Ohio 44135

Summary

NASA has set a goal to return to the Moon and to establish a sustained lunar presence. Many applicable lander and upper-stage vehicle concepts utilize cryogenic H_2 and O_2 propellants. This propellant selection enables appealing potential mission concepts wherein electricity is generated by operating a fuel cell on residual H_2 and O_2 propellants. This concept depends on the capability of the fuel cell to utilize dry, propellant-grade reactants with concentrations of up to 30 percent He present. This study consists of the evaluation of a 12-cell non-flow-through proton exchange membrane fuel cell stack of 50 cm^2 active area with passive water removal. This stack was supplied with three levels of reactant purity: >99.999, 99.1, and 70 mol%, with the remainder made up of He. The reactant humidity and flow-through rate were also assessed as performance factors, and the fuel stack repeatedly supported a load profile with current densities up to 500 mA/cm^2 (25 A). The fuel cell performed consistently over the course of testing, with cell voltages decreasing approximately 50 mV at the maximum current density when supplied with reactants with 30 percent He present.

Nomenclature

CTB	Common Test Bed
E	cell potential
exp	experimental
F	Faraday constant
n	stoichiometric factor
NFT	non-flow-through
P_E	electrical power produced by fuel cell stack
PEM	proton exchange membrane
PWR	passive water removal
RGA	residual gas analyzer
SFR	stoichiometric flow rate
theor	theoretical
USD	United States dollar
$\dot{V}$	flow rate
V_m	molar volume
Φ	stoichiometric flow rate ratio

1.0 Introduction

Current NASA space exploration plans include long-term lunar Gateway and surface missions (Ref. 1). Since it is significantly more expensive to reach the lunar surface than to simply transport to low Earth orbit, there has long been a focus on minimizing launch weight. Commercial lunar surface transport services estimate cost at 0.8 to 1.2 million USD/kg (Refs. 2 and 3). Consequently, there is considerable motivation to identify technologies compatible with the delivery system. Fuel cells present an enticing opportunity when H_2 and O_2 are selected for propellants. Reactant storage mass and volume frequently comprise the majority of the total mass and volume for fuel cell systems. There are large cost savings available when replacing a dedicated fuel cell reactant storage system with excess propellant, carried by a descent vehicle for the purpose of providing a safety margin during flight. In 2007 for the Altair lander module, residual H_2 and O_2 were considered for application as a fuel cell reactant supply in a lunar lander mission (Refs. 4 and 5). Estimated residual propellant was 3 percent of the initial quantity (Ref. 4). For the described nominal mission case, that leaves 130 kg H_2 and 706 kg O_2 unused. Since this propellant is required regardless of the inclusion of fuel cells, it may replace a fuel-cell-specific reactant storage system. At an energy conversion ratio of 2.2 kWh/kg H_2O, equivalent to 60 percent of theoretical energy, a fuel cell generates 1,746 kWh of electrical energy and 794 kg of H_2O from such a reactant quantity. This estimate assumes complete utilization of the scavenged propellant with O_2 as the limiting reactant.

There remains the question of whether modern aerospace flight fuel cells are capable of efficiently utilizing these propellants. It is common to operate terrestrial fuel cells with flow-through water management or even reforming capability on impure reactants, though this requires active ancillary components that reduce overall efficiency and increase system complexity and mass. Preferred aerospace fuel cell systems incorporate passive components to improve metrics such as specific energy and energy density (Ref. 6). It is possible to base a passive system on a flow-through or non-flow-through (NFT) fuel cell. For either design, as a result of the focus on achieving high levels of reactant utilization, electrochemical performance

is sensitive to the presence of inert species blocking the reaction surface. Because of the introduction of helium to pressurize the propellant tanks prior to an engine burn, propellant-grade gases are less pure than the reactants typically used in fuel cell development testing. In propellants, there is typically more He in O_2 than in H_2 because He is only temporarily used to pressurize H_2 during initial startup (Ref. 5). Altair lander tank pressures range from 9 to 45 psia O_2 and 17 to 33 psia H_2, which aligns well with typical proton exchange membrane (PEM) fuel cell operating pressure levels. Tank venting procedures exist that can reduce He presence in the gas supplied to a fuel cell by balancing vent duration, vent cycles, and boiloff rate. This previous analysis indicates that it is possible to reduce He to less than 0.1 mol% in H_2 and less than 1 mol% in O_2 with sufficient vent duration. This results in a marginally justifiable loss of potentially useful reactants and high levels of vaporization within the tanks. It is potentially preferable to only continue venting until obtaining 96.8 mol% H_2, remainder He, losing only 4 mol% of the total available reactant (Ref. 4). Relatively short, intermittent vent durations can limit He concentrations to less than 4 mol% with minimal vaporization. It is possible to achieve 57 mol% O_2, remainder He, losing less than 1 mol% of the total available.

It is desirable to update knowledge on the capability of current fuel cells to handle high impurity concentrations to better inform mission planning and operations. Previous testing suggests that a NFT stack can be operated with significant reactant impurity levels (Refs. 5 and 7). In those studies, no permanent damage occurred to the 32-cell, 1.5-kW unit as a result of testing with up to 95 mol% He in O_2 or 11 mol% He in H_2. A separate trial involved simultaneously supplying the stack with up to 8 mol% He in H_2 and 92 mol% He in O_2. High current densities and rapid load changes are known to be among the greatest stresses during fuel cell operation. Other than occasional current sweeps to enable development of polarization curves, all of this previous testing was conducted at a constant current. This current was selected to maintain the minimum cell voltage above 0.8 Vdc. Although it demonstrated fuel cell response to fluctuating power demands, it was not necessarily representative of a load profile that would be used in a flight mission. Also, the stack in this earlier study required occasional burping (short periods of increased reactant flow-through rate) to clear impurities when those began to impede reactant mass transfer to the membranes. Such a need is signaled by a reduction in cell voltages. Furthermore, there is concern that flow-through operation could negatively impact PEM humidity control, reducing cells voltages and potentially damaging membranes (Refs. 8 and 9).

Thus, it is of interest to update the reactant purity evaluation by examining the behavior of a modern, passive NFT design on which substantial flight-like testing had already been performed as it operates over a well-established NASA load profile.

2.0 Experimental

A passive water removal (PWR) NFT PEM fuel cell stack was utilized for this testing. The stack consists of 12 cells with 50 cm^2 active area and Nafion™ N117 (The Chemours Company FC, LLC) membranes. Previous testing on this fuel cell included launch vibration sensitivity testing and operation in a variety of stack orientations with respect to gravity. No significant performance changes were found as a result of those evaluations (Ref. 10); thus, the same hardware was deemed suitable for this evaluation. The testing was performed at Glenn Research Center on a NASA-developed fuel cell Common Test Bed (CTB). This CTB integrates manual and automated control of operating temperatures, pressures, and flow rates as well as enables remote operator control. Prior to this specific test usage, the stack had been exposed to reactants for over 51 h, completing 12 startup and shutdown cycles and 35 h supporting an electrical load at an average current density of 195 mA/cm^2. This reactant purity testing further added 98 h of reactant exposure time with 74 h under load.

Experiments were designed to study the steady-state and transient electrical performance of the fuel cell over a range of flow rates, humidification levels, and He concentrations in the H_2 and O_2 reactant gases. The studied reactant gas He concentrations are provided in Table I. Reactant gases were humidified by membrane humidifiers to a dew point of approximately 30 °C and operating pressure 50±2 psia. The humidification system is depicted in Figure 1. Dry gas flows through a calibrated mass flow meter then is supplied to the heated humidifier. At the humidifier outlet, the gas relative humidity is measured by a calibrated dew point monitor and is further heated to minimize condensation on the dew point sensor mirror then directed toward the stack under test.

TABLE I.—STUDIED HELIUM CONCENTRATIONS OF FUEL CELL REACTANTS

Concentration He in O_2, mol%	Concentration He in H_2, mol%	Reactant supply details
0	0	Baseline testing with research-grade O_2 and H_2
30	0	Vary O_2 stoichiometric flow rate; vent H_2 side only
0	30	Vary H_2 stoichiometric flow rate; vent O_2 side only
30	30	Steady-state operation
0.1	0.1	Steady-state operation

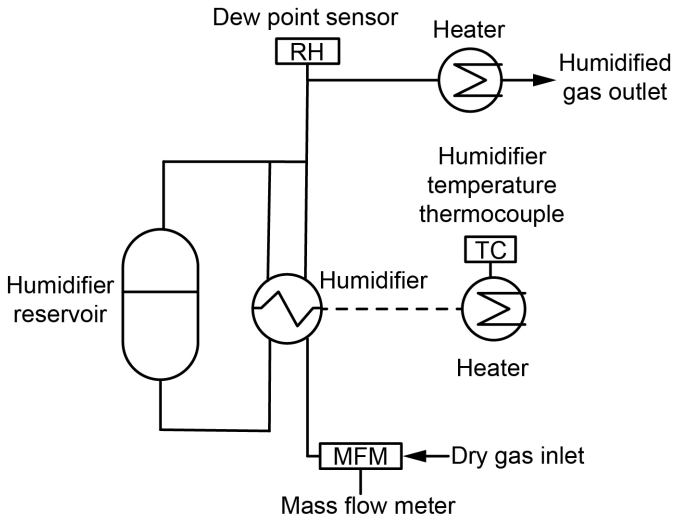

Figure 1.—Gas humidification system components. TC is thermocouple; MFM is mass flow meter; RH is relative humidity.

The humidified gas is also connected to a humidifier H_2O reservoir thereby pressurizing the static H_2O feed side of the humidifier.

Research-grade 0 mol% He reactants were supplied in a NFT configuration, with vent durations set to 10 s prompted only by any individual cell voltage decreasing below 0.6 V. To identify appropriate flow-through rates when impurities were supplied, once the stack was up to the nominal operating temperature of 60 °C and pressure was constant, tests began by manually controlling the current load then changing the reactant flow rate. For each reactant gas, the measured reactant flow rate $\dot{V}_{exp}$ was compared to the theoretical stoichiometric flow rate (SFR) $\dot{V}_{theor}$ for a given power production level to provide an SFR ratio. This SFR ratio Φ is given by Equation (1),

$$\Phi = \frac{\dot{V}_{exp}}{\dot{V}_{theor}} \tag{1}$$

The theoretical SFRs were calculated using Equation (2),

$$\dot{V}_{theor} = \frac{P_E V_m}{nEF} \tag{2}$$

where P_E is electrical power produced by the fuel cell stack, V_m is the molar volume of gas given by the ideal gas law at standard temperature and pressure, n is the stoichiometric factor equal to 2 for H_2 and 4 for O_2, E is the average individual cell potential, and F is the Faraday constant.

The current was increased in steps up to a current density maximum of 500 mA/cm², and the reactant flow rates were adjusted to obtain stable stack performance. This was done to verify stack health, establish appropriate rotameter flow control setpoints, and ensure sufficient purging of reactant supply lines from the facility supply connection through the CTB to the stack. Reactants were not recirculated in this system and were vented from the facility after exiting the fuel cell stack, though it is possible that a flight configuration could incorporate this capability.

With those conditions satisfied, a 2-h load profile commenced, preceded and followed by current sweeps. Additional measurements and observations included power production capability with different combinations of inert concentration and SFR ratio as well as venting frequency for a given SFR. Helium crossover was monitored through periodic sampling of the gases exiting the fuel cell stack. Samples were directed to a residual gas analyzer (RGA). Following tests requiring higher SFR ratios, the stack was also monitored for product H_2O loss to vented gas rather than to the dedicated H_2O collection system to verify the internal stack H_2O separation mechanisms continued to function normally.

3.0 Results and Discussion

3.1 Performance Over Load Profile

Figure 2 depicts fuel cell operation when supplied with high-purity reactants. Even though the stack was operated in a NFT mode as evidenced by the SFR ratios near 1, impurities were minimal enough during the load profile that stack voltage performance was very stable. The occasional spikes in H_2 SFR ratio represent vents due to an individual cell voltage decreasing below the minimum cell potential vent setpoint, typically 0.6 Vdc. The effect of 30 mol% He impurity in H_2 is displayed in Figure 3. Whereas the O_2 SFR ratio remained at 1, H_2 SFR ratio varied from 2 to 8 during the load profile. This satisfied the minimum cell voltage constraints, but the total stack voltage still decreased during the constant-current sections of the profile. Excess humidification and H_2O condensation in sections of the H_2 reactant supply system may have impaired performance during this test run. Installing precisely placed condensate traps between the humidifier and fuel cell stack appeared to remedy the issue. The fuel cell performance was more consistent with research-grade H_2 and 30 mol% He in O_2 as shown in Figure 4. The load profile was successfully completed with an O_2 SFR ratio near 4. When 30 mol% He is present in both reactants, the stack operated with minimally affected performance, with SFR ratios generally between 3 and 4 as presented in Figure 5. If impurity concentration is reduced to 0.1 mol% He in both reactants, similar performance can be obtained with SFR ratios around 2 as established in Figure 6.

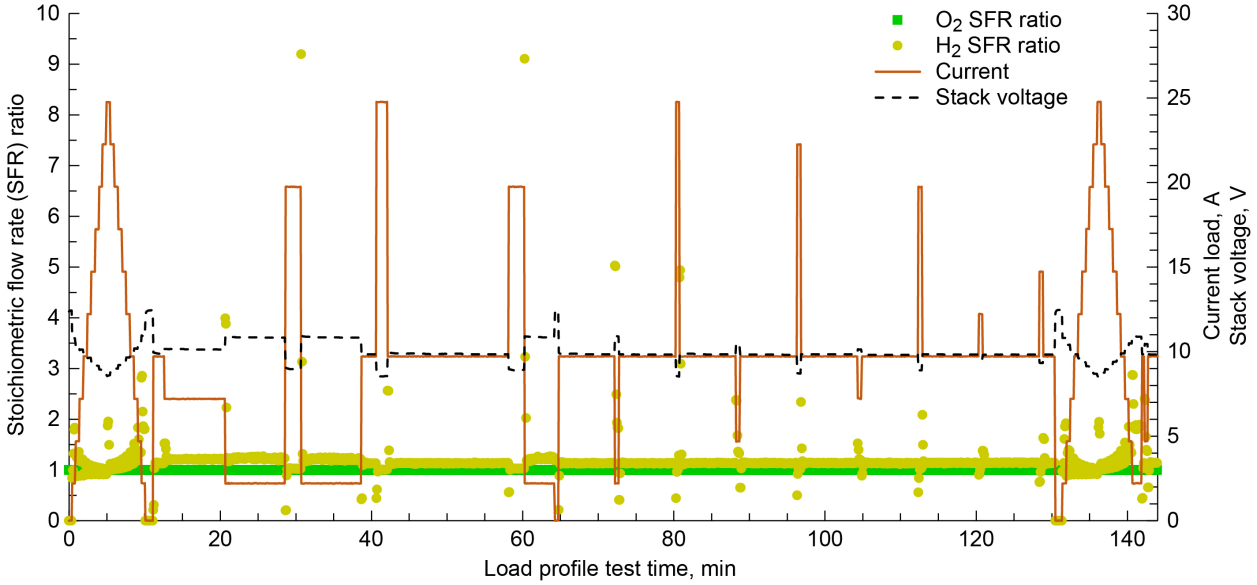

Figure 2.—PEM fuel cell stack voltage performance and reactant flow rates operating over load profile while supplied with research-grade O_2 and H_2 reactants.

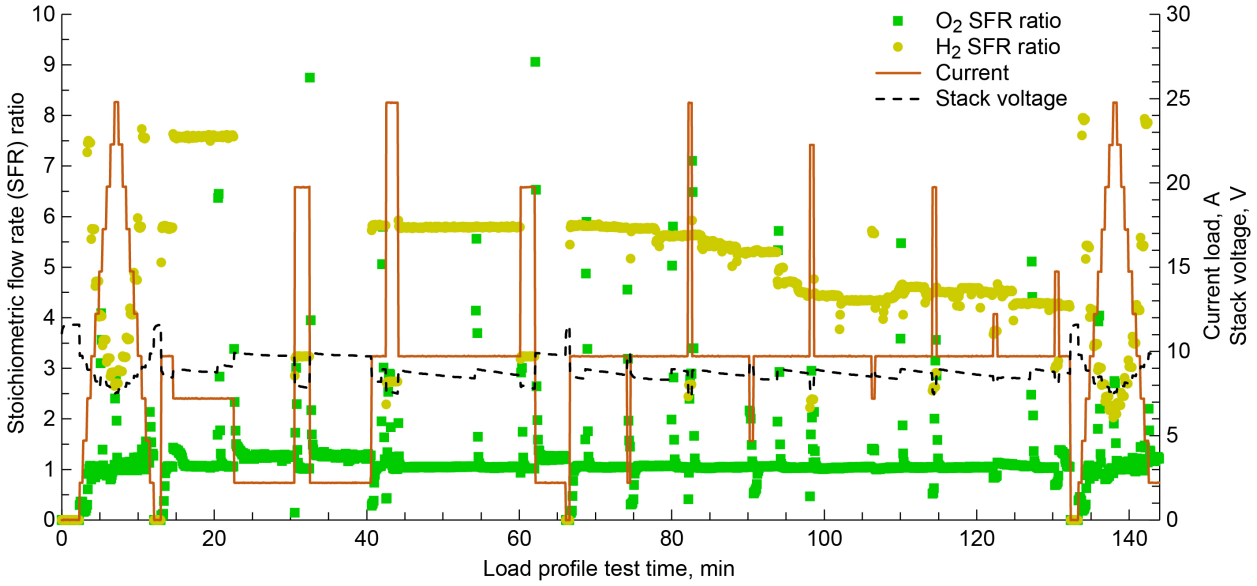

Figure 3.—PEM fuel cell stack voltage performance and reactant flow rates operating over load profile while supplied with research-grade O_2 and with H_2 containing 30 mol% He.

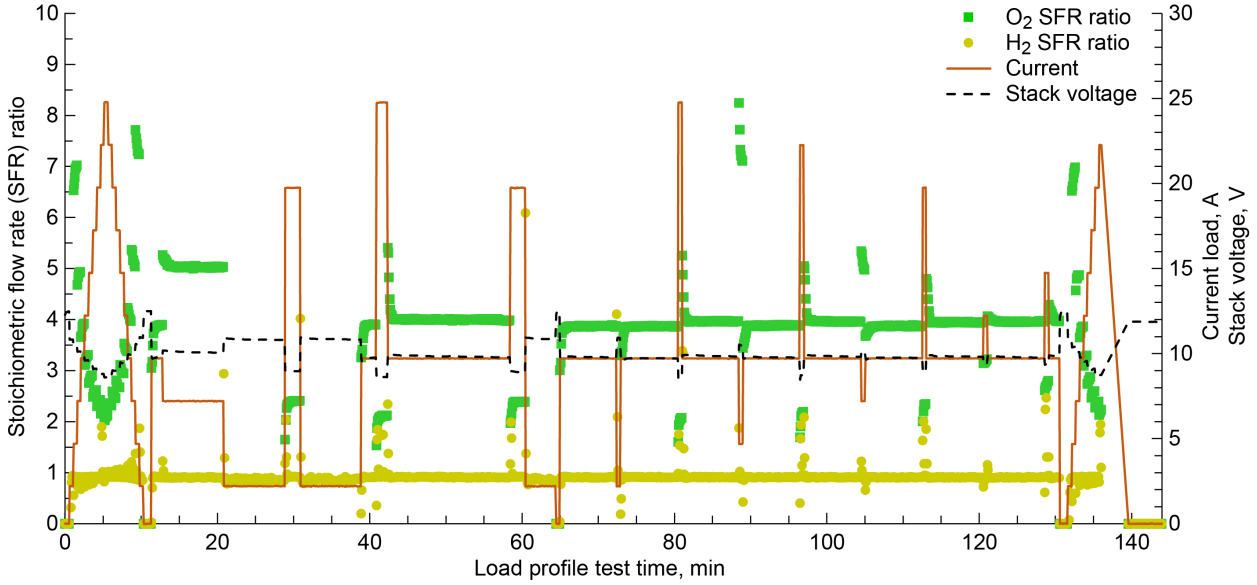

Figure 4.—PEM fuel cell stack voltage performance and reactant flow rates operating over load profile while supplied with research-grade H_2 and with O_2 containing 30 mol% He.

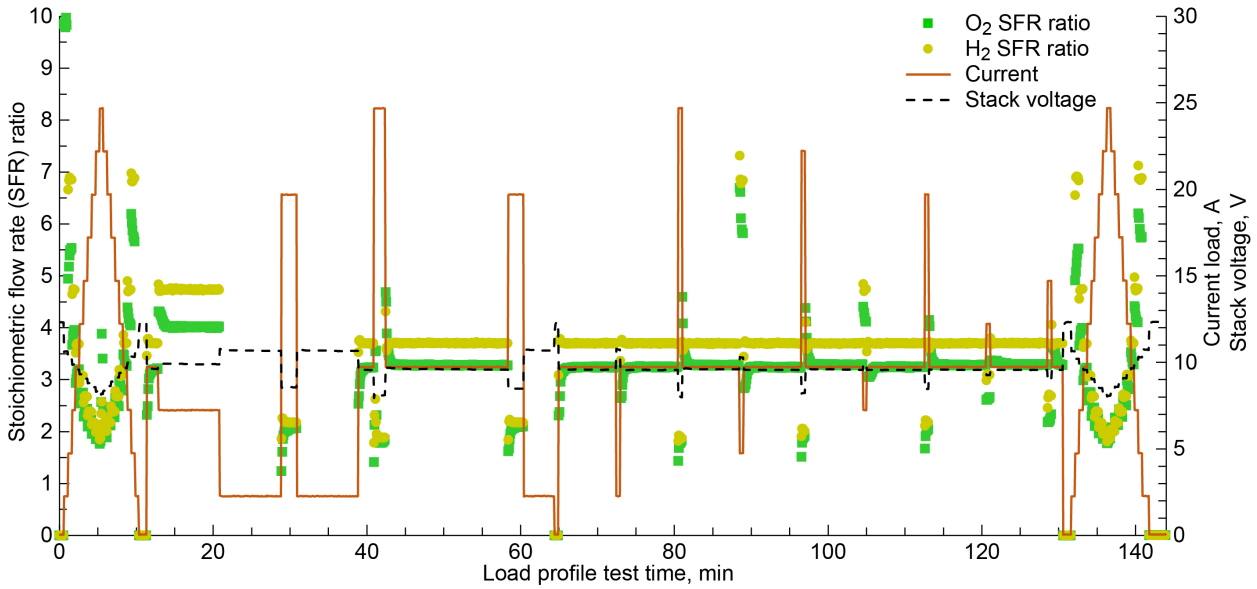

Figure 5.—PEM fuel cell stack voltage performance and reactant flow rates operating over load profile while supplied with O_2 with 30 mol% He and H_2 with 30 mol% He.

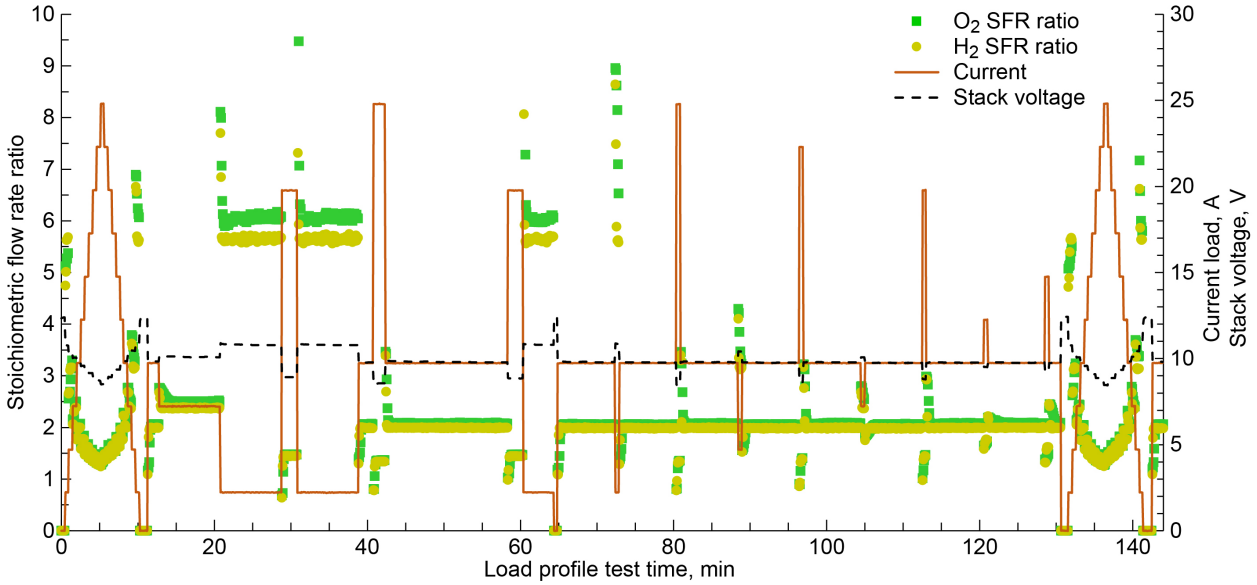

Figure 6.—PEM fuel cell stack voltage performance and reactant flow rates operating over load profile while supplied with O_2 and H_2, each containing 0.1 mol% He.

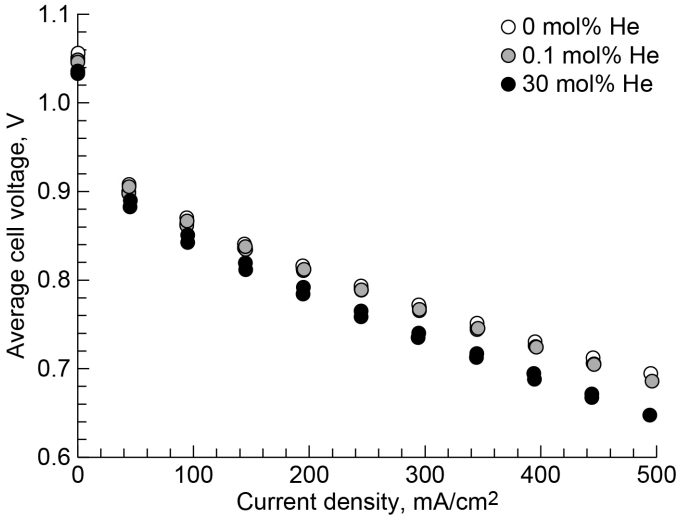

Figure 7.—PEM fuel cell polarization curve comparing effect of He impurity in both H_2 and O_2 reactants.

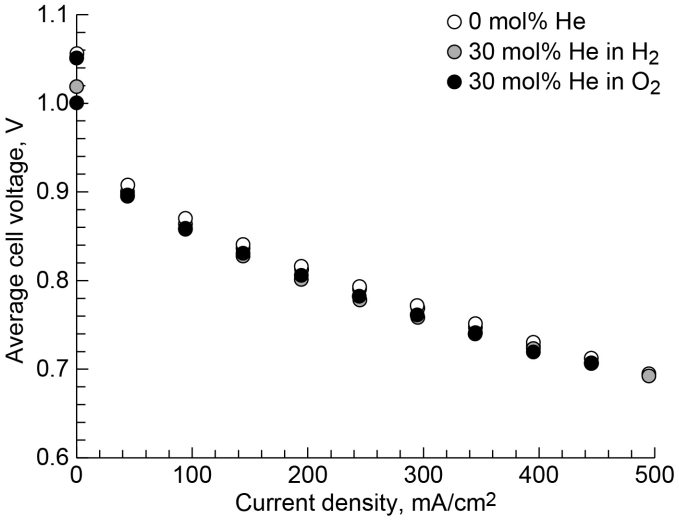

Figure 8.—Polarization curve comparing effect of He in either H_2 or O_2 reactant gas.

3.2 He Effects and Crossover

Figure 7 shows the polarization curves up to 500 mA/cm^2 for 0, 0.1, and 30 mol% He in both reactants. At that maximum current density, there was a 9 mV reduction in average cell voltage with 0.1 mol% He and a 47 mV decrease with 30 mol% He. In Figure 8, the polarization curves are presented for 0 mol% He in both reactants, 30 mol% He in H_2 and research-grade O_2, and 30 mol% He in O_2 and research-grade H_2. Comparing the trials of 30 mol% He in H_2 while O_2 was research grade with the reverse-case trials of 30 mol% He in O_2 and research-grade H_2, the average cell potential at 500 mA/cm^2 was negligibly different at only 1 mV less. Additionally, the case that produced the higher average cell voltage varied at lower current loads. There is no preference here for where the He originates. This contradicts previous NASA testing and the theory that because of the greater difference in atomic mass between He and O_2 compared to H_2, He is preferentially removed during O_2 venting (Ref. 7).

Over three runs through the standard load profile with research-grade reactants, H_2 venting and O_2 venting were each initiated once every 22 min on average, based on cell voltage readings. When 0.1 mol% He was supplied in both reactants, the vent intervals averaged approximately once every 15 min. When supplying 30 mol% He in H_2 to the stack, H_2 venting occurred more frequently than once every 9 min on average for each of the four runs. When supplying 30 mol% He in O_2 to the stack, O_2 side venting occurred more frequently than once every 10 min on average for each of the three runs. Average vent intervals reduced for both reactants even if only one was supplied with an impurity. During 18 h of testing over four trials with 30 mol% He in H_2 and research-grade O_2, average O_2 vent intervals did not exceed 6 min for any trial, even if set in a flow-through configuration. This suggests crossover of the He through the membrane to the other side of the fuel cell.

High-temperature filaments in the RGA can split atoms for measurement, leading to the presence of monatomic and diatomic forms. Evaluating RGA measurements of anode outlet H_2 samples from test runs using research-grade H_2 while O_2 contained 30 mol% He, like the result shown in Figure 9, strong peaks are visible at atomic mass units 1 and 2, representing H_2, while a smaller 4 amu peak represents He. This RGA result is clear evidence of He diffusion through the membrane against proton conduction. There are negligible peaks at 14 and 28 amu, signifying the presence of N_2 and at 18 and 19 amu for H_2O. O_2 cathode outlet gas samples were also analyzed, an example of which is provided in Figure 10 for a test run during which 30 mol% He was only present in the H_2 supply gas. Although the O_2 peaks at 16 and 32 amu are the greatest, there is evidence of He at 4 amu. The remainder of the peaks at 1, 17, 18, and 19 amu suggest the presence of H_2O that cannot be completely removed from the sample. H_2O is generated on the O_2 side of the fuel cell membranes, and the RGA measurement process fractionates the molecule into constituent groups. This minimal H_2O quantity is evidence of the stack internal PWR effectiveness even during flow-through operation.

3.3 Performance Degradation

Reactants were successfully humidified to dew points near 30 °C, as observed in effluent reactants. The humidification work was somewhat limited by the membrane area of the gas humidifiers and lack of automated reactant flow control to adjust the flow rate when current varied. Precise humidification control is likely to become more important for fuel cell membrane durability over longer operational durations.

Following the trials with impurities, a polarization curve was again completed with research-grade reactants. For current densities ranging from 0 to 500 mA/cm^2, the resulting power production is shown in Figure 11 alongside both initial performance when the stack was new and performance after the baseline tests with research-grade reactants, immediately prior to supplying lower purity reactants. At higher current densities, the power production appears to diminish over time as a result of decreased average cell voltages. This degradation is distinct from the temporary cell voltage suppression caused by inert species crowding reactants near the reaction surface

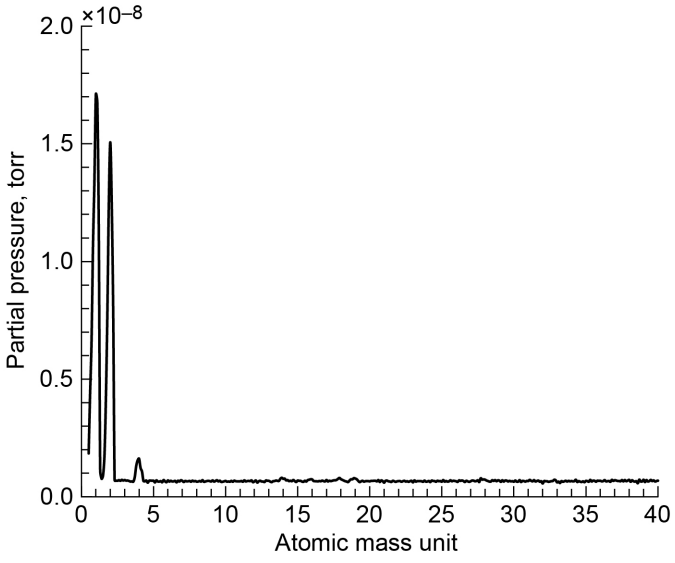

Figure 9.—Residual gas analyzer (RGA) anode outlet sample from PEM fuel cell supplied with research-grade H_2 with O_2 containing 30 mol% He.

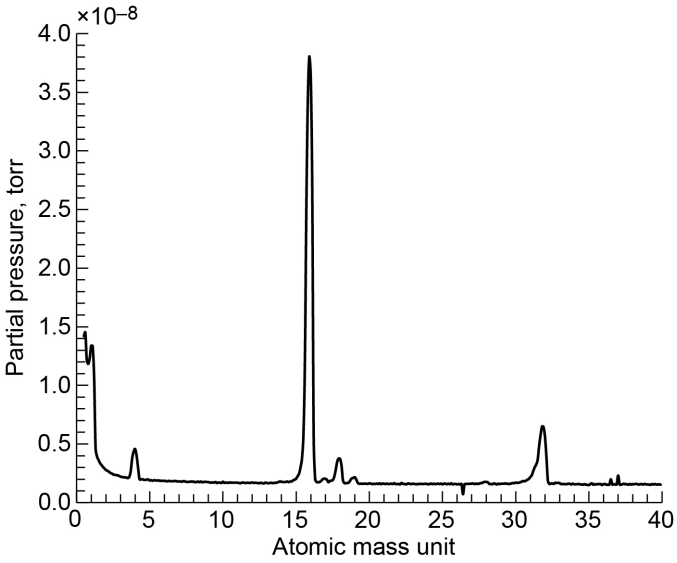

Figure 10.—Residual gas analyzer (RGA) cathode outlet sample from PEM fuel cell supplied with research-grade O_2 with H_2 containing 30 mol% He.

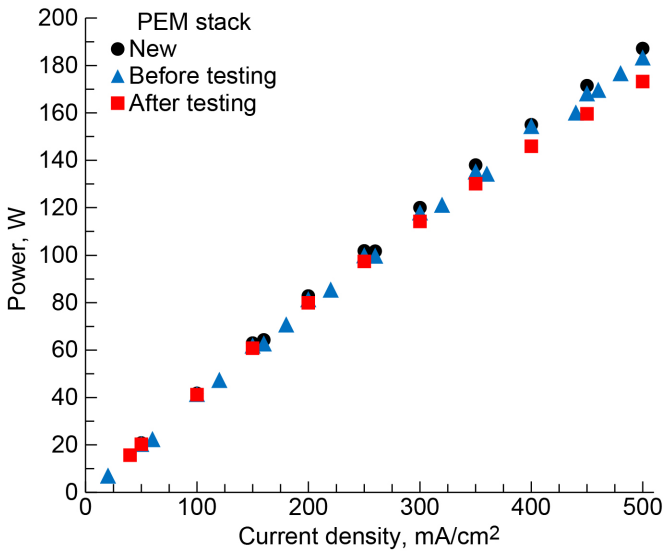

Figure 11.—Total PEM fuel cell stack power production versus current density when stack is new, before use in He impurity testing, and after use in He impurity testing.

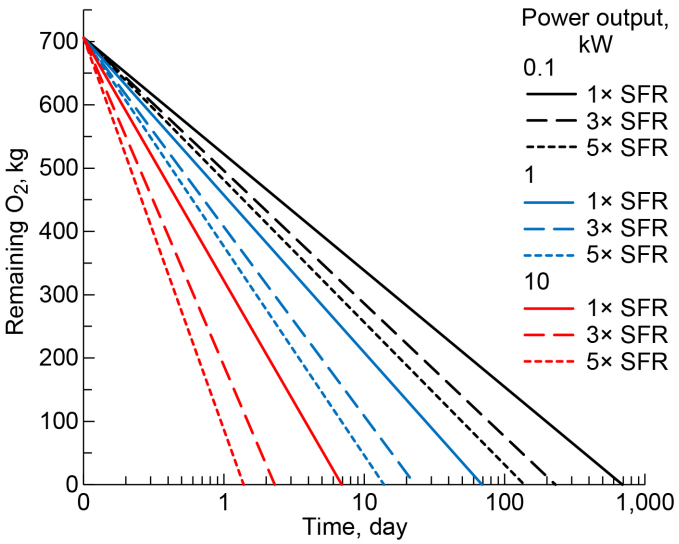

Figure 12.—Projected O_2 fuel cell reactant availability over time for different combinations of power output and flow rate (multiples of stoichiometric flow rate (SFR)).

and effectively reducing the reactant partial pressure. At 500 mA/cm^2, overall power production decreased approximately 5 percent relative to the initial power output over the duration of impurities testing.

The tested stack degraded at a similar rate when operating with research-grade reactants. Over the first 51 h of operation, solely performed with research-grade reactants, the average cell voltage degradation rate was 0.2 μV/h. During the 98 h of testing required for this study, the degradation rate was 0.6 μV/h. With the existing test data from the single stack, it is not possible to determine if this rate increase is due to periods of operation without humidification, higher impurity concentrations, normal ageing and deterioration of this particular stack design, or some other factor. Regardless, for one-time-use mission concepts of shorter durations, this level of degradation is minimally impactful.

3.4 Reactant Utilization

Considering the results presented in this study in the context of a lunar lander concept, it is constructive to evaluate how a NFT fuel cell would operate within such a mission. Since O_2 is the stoichiometrically limiting reactant, Figure 12 is constructed based on utilization of that species in a fuel cell operating at 0.818 Vdc and 200 mA/cm^2 on humidified reactants. In addition to the nominal SFR ratio, venting at an SFR of 10 is assumed to occur for 10 s every 10 min (1.7 percent of the time). For SFR ratios of 1, 3, and 5 at constant 0.1, 1, and 10 kW power levels, this figure shows the amount of O_2 that remains over time. These increasing SFRs were chosen to align with the needed flow rates to operate a fuel cell with 0, 0.1, and 30 mol% He supplies. The availability of higher purity reactant enables lower SFRs and greater reactant utilization so that less of the supply is wasted. Thus, a 10-kW stack could operate for nearly 7 days with an SFR ratio of 1 but would be limited to approximately 33 h when the ratio is 5. This demonstrates the benefit and importance of the preferential venting techniques previously evaluated by NASA personnel or development of reactant recovery and purification technologies (Refs. 4 and 5).

4.0 Conclusions

As a result of costs near 1 million USD/kg to deliver payloads to the lunar surface, the minimization of launch mass is critical. There exists substantial opportunity to generate electricity with negligible additional mass by operating a fuel cell on residual H_2 and O_2 propellants when available within a lander. This report detailed the evaluation of a 12-cell proton exchange membrane fuel cell stack with 50 cm^2 active area, which incorporated passive water removal and non-flow-through reactant management technology, supplied with various He concentrations up to 30 mol%. The fuel cell operated consistently over all concentration levels with effective H_2O management but required flow-through operation when testing included He. The fuel cell internal product water removal system remained effective at separating liquid water even with flow through the O_2 cavity at 2 to 3 times the stoichiometric flow rate (SFR). Individual cells exhibit an average cell voltage reduction of 9 mV with 0.1 mol% He and 47 mV with 30 mol% He in both reactants at 500 mA/cm^2. The cell voltage was more sensitive to total quantity of He supplied as opposed to its presence in either H_2 or O_2. It did not matter which reactant

carried the He; it appears that He readily crossed through the membrane in both directions.

References

1. National Aeronautics and Space Administration: Moon to Mars. 2018. https://www.nasa.gov/feature/nasa-unveils-sustainable-campaign-to-return-to-moon-on-to-mars Accessed April 15, 2021.
2. PTScientists GmbH: Starter Payload User Guide. Mission to the Moon PTS_MttM_Starter_PUG_001_V01, 2018.
3. Astrobotic: Lunar Delivery Peregrine Lunar Lander: Payload User's Guide. Version 4, 2020. www.astrobotic.com Accessed April 16, 2021.
4. Polsgrove, Tara; Button, Robert; and Linne, Diane: Altair Lunar Lander Consumables Management. AIAA 2009–6589, 2009.
5. Linne, Diane L., et al.: Feasibility of Scavenging Propellants From Lander Descent Stage to Supply Fuel Cells and Life Support. AIAA 2009–6511, 2009.
6. Hoberecht, Marc A.: A Comparison of Flow-Through Versus Non-Flow-Through Proton Exchange Membrane Fuel Cell Systems for NASA's Exploration Missions. NASA/TM—2010-216107, 2010. https://ntrs.nasa.gov
7. Loyselle, P., et al.: NASA Glenn Research Center, Cleveland, Ohio, internal report, 2009.
8. Williams, Minkmas V.; Kunz, H. Russell; and Fenton, James M.: Operation of Nafion®-Based PEM Fuel Cells With No External Humidification: Influence of Operating Conditions and Gas Diffusion Layers. J. Power Sources, vol. 135, nos. 1–2, 2004, pp. 122–134.
9. Yang, B.; Fu, Yongzhu; and Manthiram, A.: Operation of Thin Nafion-Based Self-Humidifying Membranes in Proton Exchange Membrane Fuel Cells With Dry H_2 and O_2. J. Power Sources, vol. 139, no. 1, 2004, pp. 170–175.
10. Gilligan, Ryan P., et al.: Structural Dynamic Testing for Air-Independent Proton Exchange Membrane (PEM) Fuel Cell Technologies for Space Applications. ASME 2019 International Mechanical Engineering Congress and Exposition, Paper No. IMECE2019–11691, 2019.